Electronic Supplementary Information to:

Mn_2C MXene Functionalized by Oxygen is a Semiconducting Antiferromagnet and Efficient Visible Light Absorber

Jiří Kalmár and František Karlický*

Department of Physics, Faculty of Science, University of Ostrava, 30. dubna 22, 7013 Ostrava, Czech Republic. Tel: +420 553 46 2155; E-mail: frantisek.karlicky@osu.cz

Contents

S1 Magnetic Configurations

S1.1 Geometries - Figures

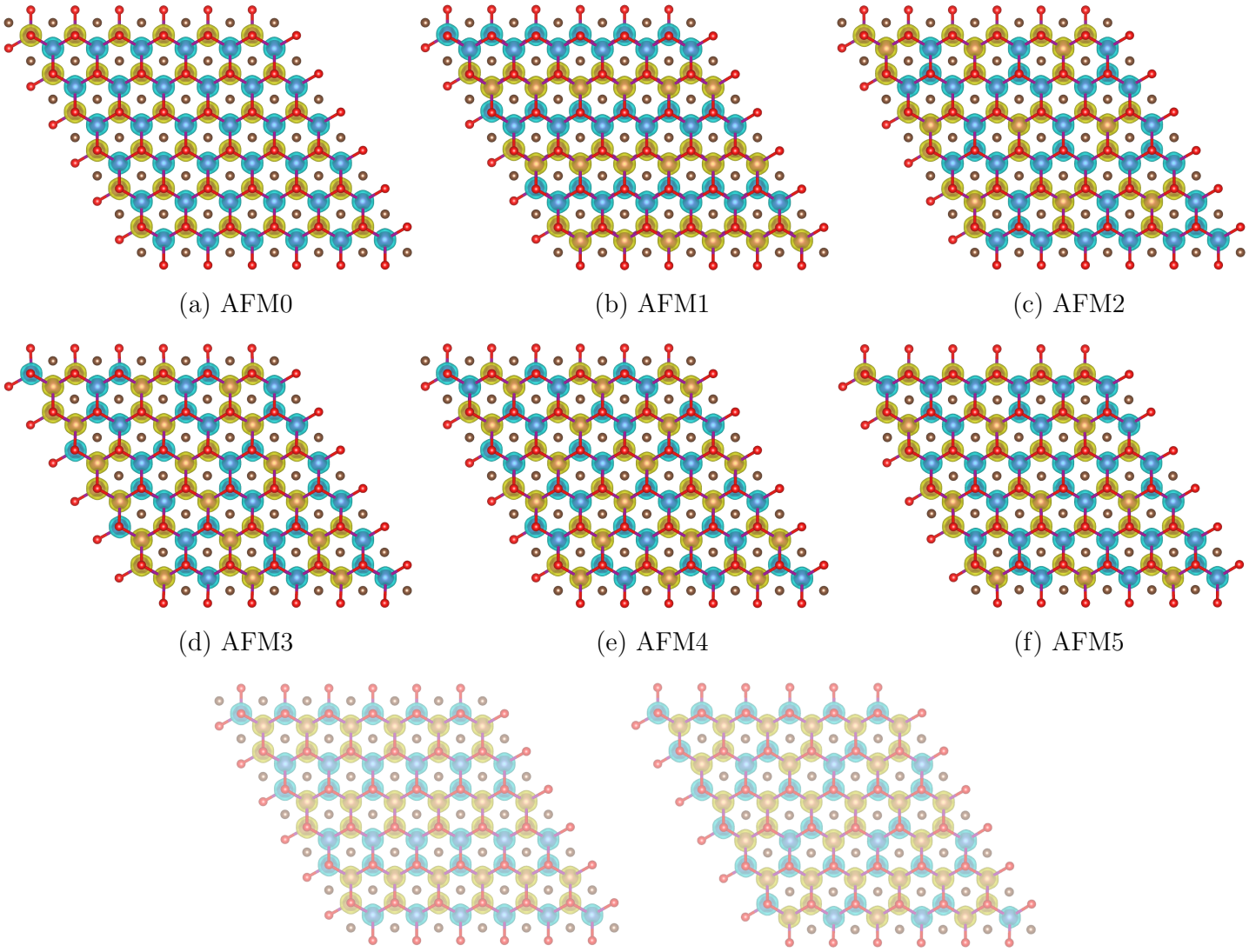

(a) AFM0 (b) AFM1 (c) AFM2

(d) AFM3 (e) AFM4 (f) AFM5

(g) AFM6=AFM4 (h) AFM7=AFM5

Figure S1: All antiferromagnetic (AFM) spin conformations of the $2 \times 2 \times 1$ Mn_2CO_2 MXene for the T1 geometry. The greyed-out conformations turned out to be identical with a different spin state. Different colors correspond to spin density - the residual spin-up (yellow) or spin-down (blue) on each transition metal.

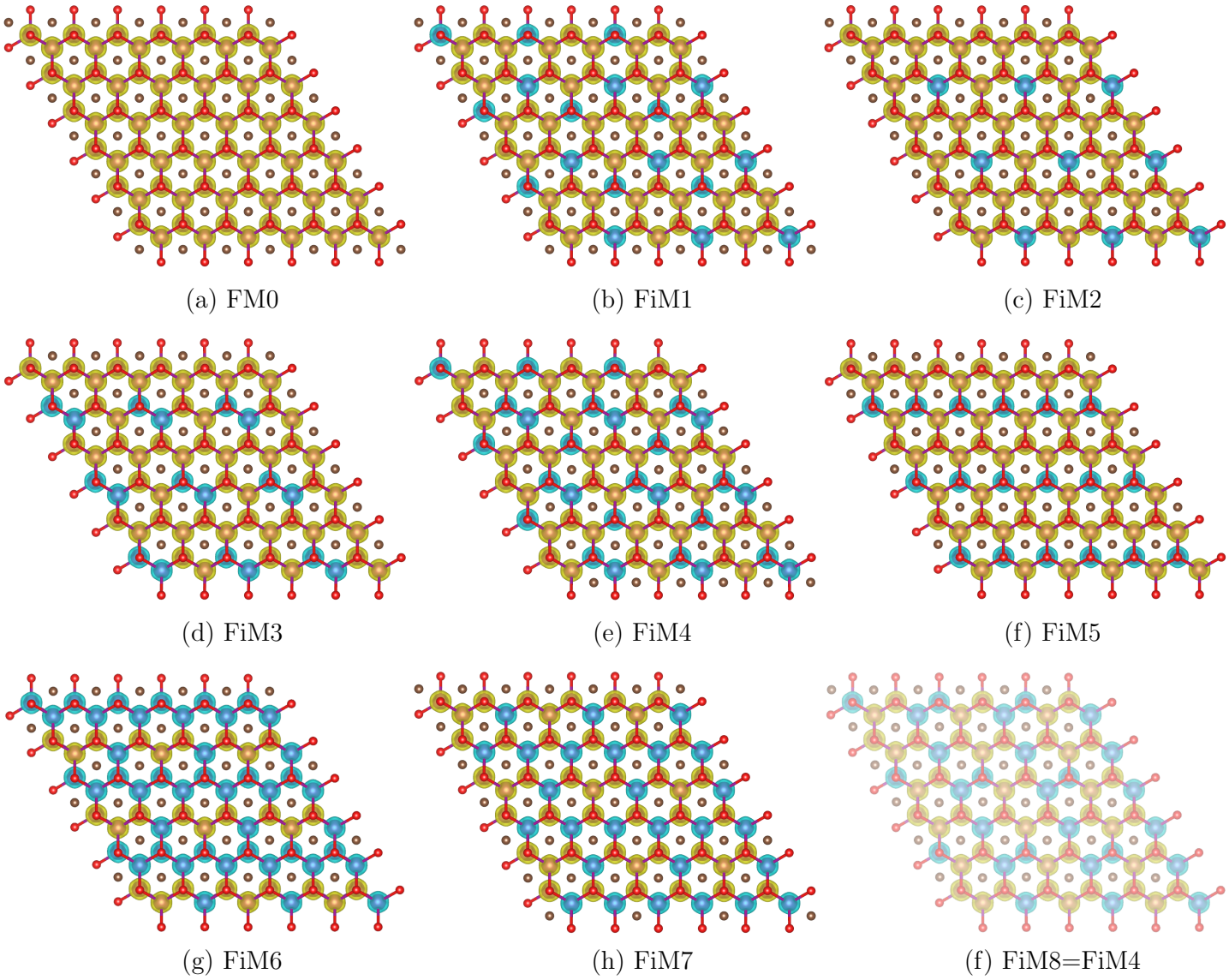

(a) FM0 (b) FiM1 (c) FiM2

(d) FiM3 (e) FiM4 (f) FiM5

(g) FiM6 (h) FiM7 (f) FiM8=FiM4

Figure S2: Ferromagnetic (FM) and all ferrimagnetic (FiM) spin conformations of the $2 \times 2 \times 1$ Mn_2CO_2 MXene for the T1 geometry. The greyed-out conformations turned out to be identical with a different spin state. Different colors correspond to spin density - the residual spin-up (yellow) or spin-down (blue) on each transition metal.

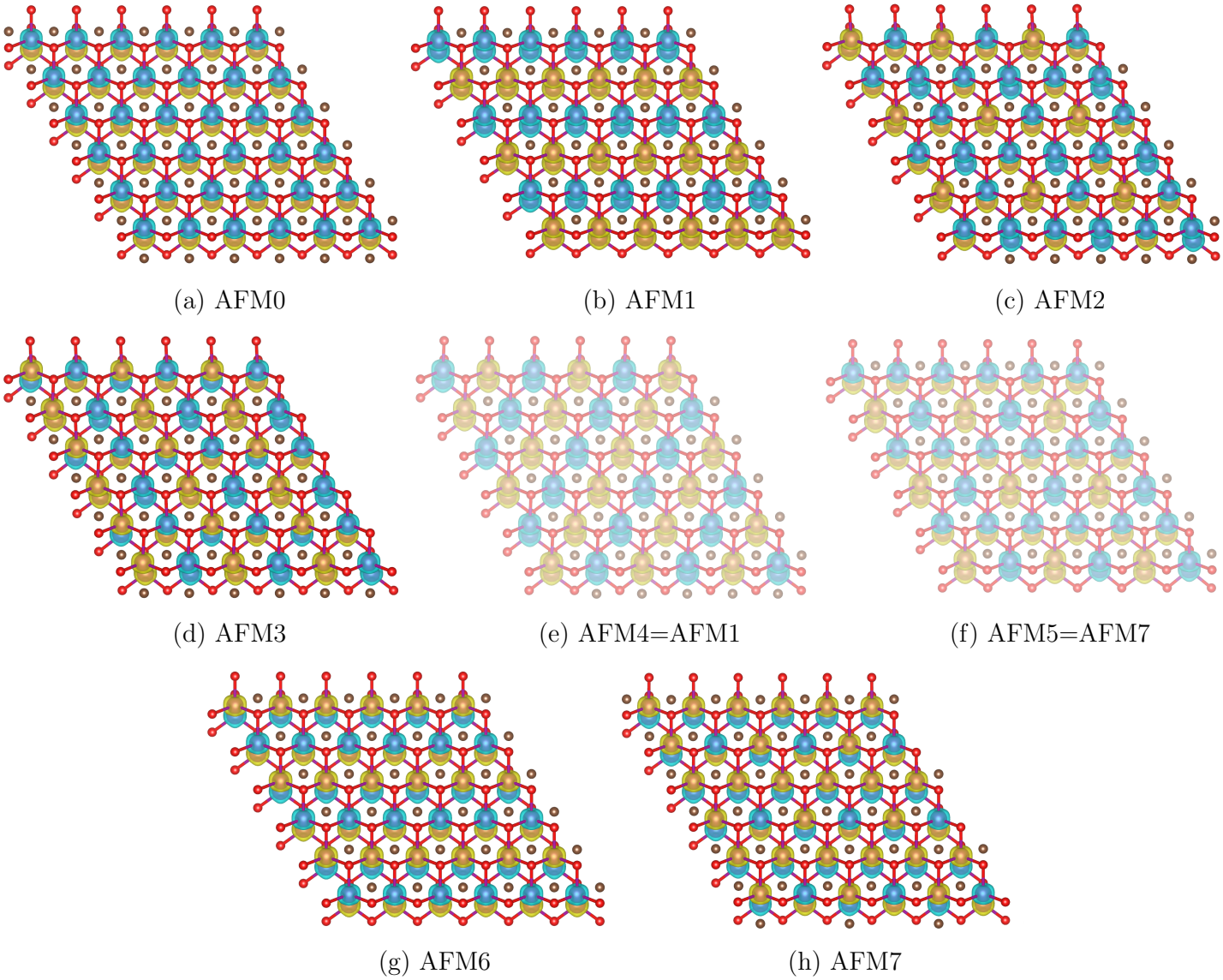

(a) AFM0 (b) AFM1 (c) AFM2

(d) AFM3 (e) AFM4=AFM1 (f) AFM5=AFM7

(g) AFM6 (h) AFM7

Figure S3: All antiferromagnetic (AFM) spin conformations of the $2 \times 2 \times 1$ Mn_2CO_2 MXene for the H1 geometry. The greyed-out conformations turned out to be identical with a different spin state. Different colors correspond to spin density - the residual spin-up (yellow) or spin-down (blue) on each transition metal.

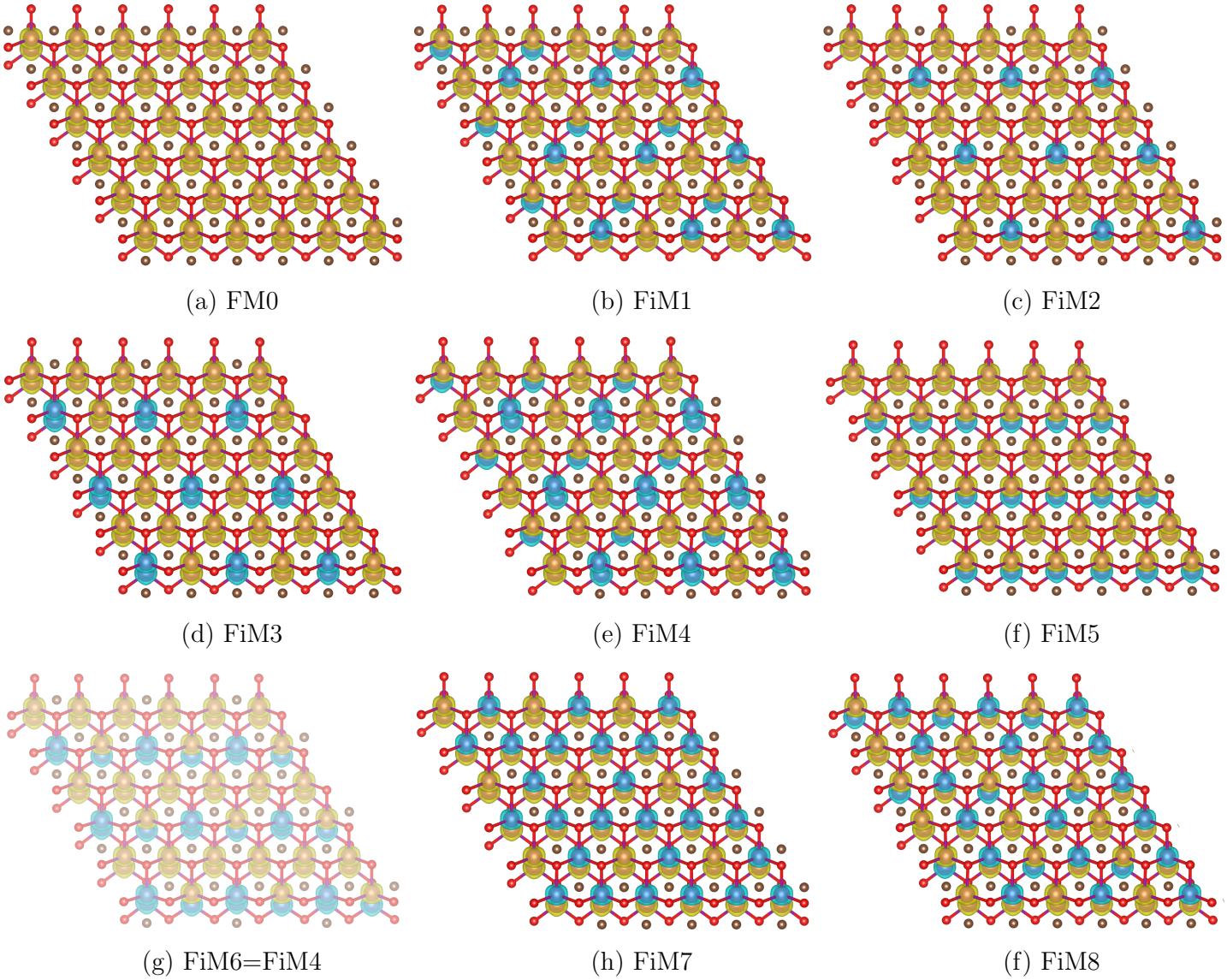

(a) FM0 (b) FiM1 (c) FiM2

(d) FiM3 (e) FiM4 (f) FiM5

(g) FiM6=FiM4 (h) FiM7 (f) FiM8

Figure S4: Ferromagnetic (FM) and all ferrimagnetic (FiM) spin conformations of the $2 \times 2 \times 1$ Mn_2CO_2 MXene for the H1 geometry. The greyed-out conformations turned out to be identical with a different spin state. Different colors correspond to spin density - the residual spin-up (yellow) or spin-down (blue) on each transition metal.

S1.2 Energetics and Stability

Firstly, we did structural optimizations and ground-state calculations on all 28 conformers at the level of PBE density functional. The results show, that even though spin conformation H1-AFM6 is the energy ground-state, the energy differences between individual conformations are very small, not exceeding 0.25 eV, with the difference between the first two being only 27 meV. From the reported electronic band gaps we can also see that some conformations exhibit semiconducting behavior while others have been shown to be metallic.

From the results of electronic band gaps, we can see that the isomer H1-AFM1 should exhibit metallic behavior. In the close-up part of its PBE band structure (ESI Fig. S6b) we can see that the conduction band clearly crosses the Fermi energy and therefore the material is at the PBE level of theory classified as a metal. It is however necessary to consider the nature of PBE and its band gap determination. DFT is well known for underestimating the band gap and also materials that were wrongly predicted to be gapless have exhibited a non-zero gap with the use of higher tier of exchange-correlation functionals. Therefore we needed to continue at the higher level of theory.

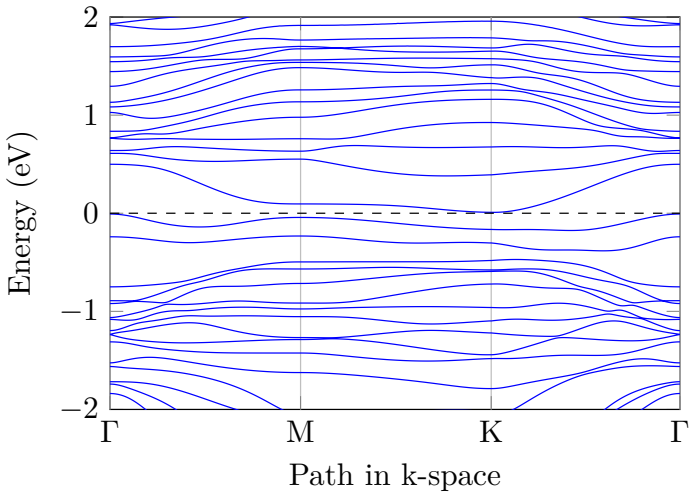

Figure S5: PBE band structure of H1-AFM3. The Fermi energy is set to zero.

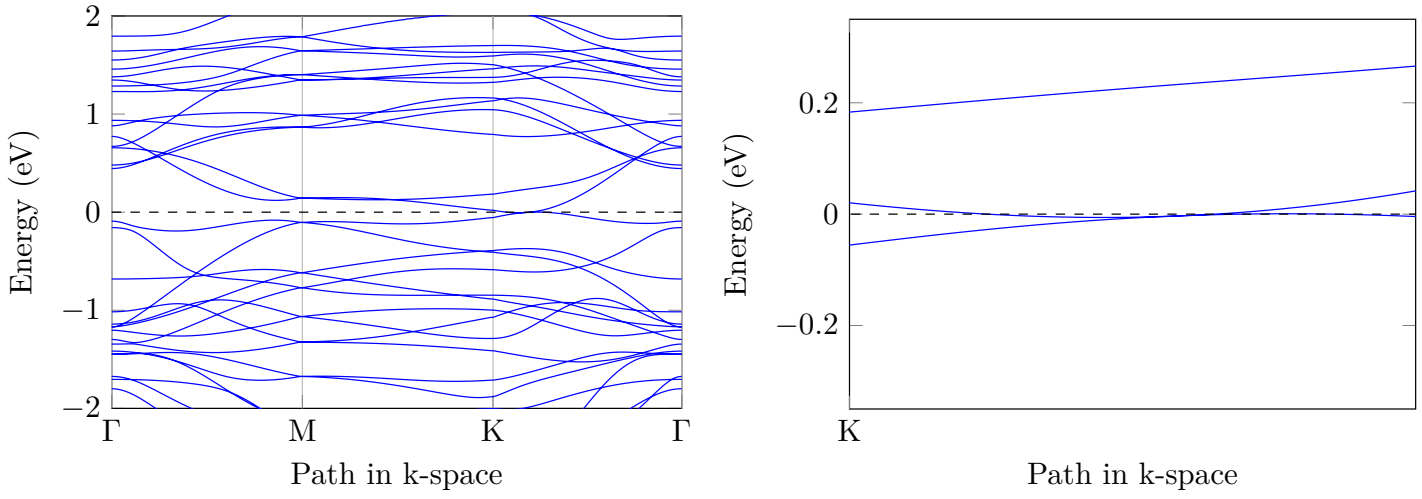

(a) (b)

Figure S6: PBE bandstructure of (a) H1-AFM1 and (b) a close-up area near the Fermi energy, which is set to zero.

Table S1: Relative energies (R.E.) per unit cell (1×1) at the level of PBE functional for T1 and H1 isomers for all 28 calculated spin configurations and their direct and indirect band gaps. Solutions without band gaps exhibit metallic behavior. For spin-polarized FM and FiM states, the lower value of the band gap is reported. All energies are presented in eV.

Phase	R.E.	E_g^{dir}	E_g^{indir}
H1-AFM6	0.0000	0.30	0.18
H1-AFM3	0.0266	0.16	0.05
H1-AFM1	0.0282	-	-
H1-FiM8	0.0398	0.29	0.04
H1-FiM4	0.0430	-	-
T1-AFM1	0.0521	0.37	0.24
H1-AFM2	0.0550	0.25	0.12
H1-AFM7	0.0579	0.53	0.51
H1-FiM3	0.0659	-	-
H1-FiM1	0.0683	0.28	0.08
H1-FiM5	0.0895	0.14	0.14
T1-FiM6	0.0912	0.26	0.18
T1-AFM3	0.0930	0.28	0.19
T1-AFM2	0.0981	0.58	0.55
H1-FiM7	0.1052	0.34	0.26
H1-FiM2	0.1107	0.22	0.19
T1-AFM4	0.1181	0.26	0.09
T1-FiM3	0.1185	0.30	0.21
T1-FiM4	0.1209	0.29	0.14
T1-AFM5	0.1234	0.40	0.37
H1-AFM0	0.1426	0.66	0.40
T1-FiM5	0.1428	0.46	0.31
H1-FM0	0.1438	0.51	0.20
T1-FiM7	0.1565	0.58	0.54
T1-FiM1	0.1577	0.26	0.06
T1-FiM2	0.1663	0.41	0.41
T1-AFM0	0.2065	0.70	0.64
T1-FM0	0.2225	0.32	0.25

Table S2: Relative energies (R.E.) per unit cell (1×1) at the level of meta-GGA functional SCAN for T1 and H1 isomers for all 28 calculated spin configurations and their direct and indirect band gaps. For spin-polarized FM and FiM configurations, the lower value of the band gap is reported. The lattice constant a of all spin solutions corresponds to the ground-state T1-AFM1. The last three columns show the thermodynamical probability, $\exp(-E/kT)$, of a given state at temperature $T = 10$, 100 and 300 K. All energies are presented in eV.

Phase	R.E.	$E_{\mathrm{g}}^{\mathrm{indir}}$ ($E_{\mathrm{g}}^{\mathrm{dir}}$)	10 K [%]	100 K [%]	300 K [%]
T1-AFM1	0.000	0.73 (0.92)	100.00	67.03	16.79
T1-FiM6	0.017	0.73 (0.87)	0.00	9.31	8.69
H1-AFM1	0.018	0.26 (0.41)	0.00	7.91	8.23
T1-AFM2	0.023	0.86 (1.13)	0.00	4.53	6.84
T1-AFM3	0.024	0.64 (1.03)	0.00	4.04	6.58
T1-FiM3	0.031	0.66 (0.66)	0.00	1.89	5.11
T1-AFM4	0.037	0.58 (0.73)	0.00	0.92	4.02
T1-FiM4	0.037	0.53 (0.70)	0.00	0.90	4.00
T1-AFM5	0.041	0.74 (0.92)	0.00	0.58	3.45
H1-FiM4	0.042	0.28 (0.48)	0.00	0.54	3.37
H1-FiM3	0.043	0.28 (0.51)	0.00	0.48	3.24
T1-FiM5	0.046	0.64 (0.76)	0.00	0.34	2.89
H1-AFM3	0.047	0.40 (0.79)	0.00	0.31	2.78
H1-AFM2	0.049	0.38 (0.78)	0.00	0.23	2.55
T1-FiM1	0.049	0.37 (0.52)	0.00	0.22	2.49
H1-FiM1	0.053	0.37 (0.65)	0.00	0.14	2.13
H1-FiM5	0.056	0.52 (0.75)	0.00	0.11	1.96
T1-FiM2	0.056	0.54 (0.54)	0.00	0.11	1.96
H1-AFM6	0.057	0.58 (1.03)	0.00	0.09	1.88
H1-FiM8	0.057	0.41 (0.88)	0.00	0.09	1.85
T1-FiM7	0.057	0.83 (0.95)	0.00	0.09	1.84
H1-FiM2	0.060	0.48 (0.55)	0.00	0.06	1.63
H1-FiM7	0.067	0.50 (0.90)	0.00	0.03	1.24
H1-FM0	0.069	0.45 (0.45)	0.00	0.02	1.17
H1-AFM7	0.069	0.67 (1.07)	0.00	0.02	1.17
T1-FM0	0.079	0.47 (0.47)	0.00	0.01	0.79
H1-AFM0	0.082	0.70 (1.06)	0.00	0.00	0.70
T1-AFM0	0.085	1.25 (1.11)	0.00	0.00	0.64

S1.3 Molecular Dynamics

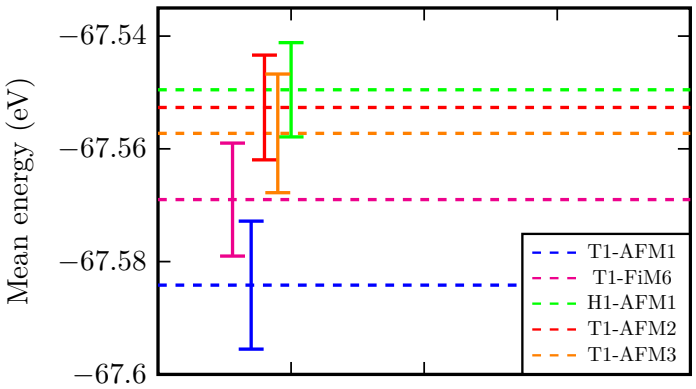

Figure S7: Mean energies from SCAN *ab initio* molecular dynamics simulations with a standard deviation of the energies for the top five most favorable spin conformations of Mn_2CO_2. Mean energies correspond to the 1×1 unit cell. Calculations were conducted on 6×6 supercells with 2 fs time steps for a total of 650 steps.

S1.4 Phonon dispersion spectra

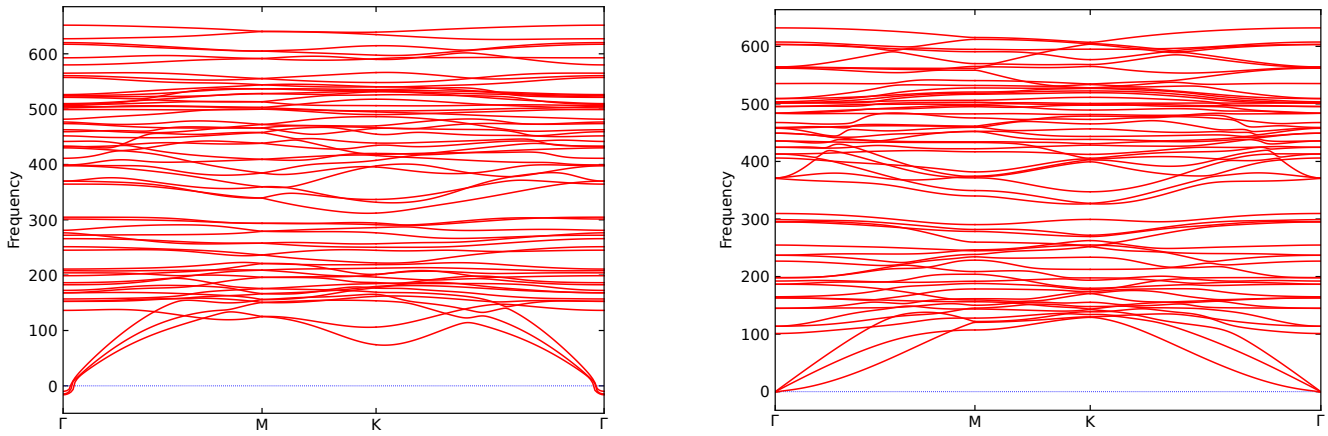

(a) (b)

Figure S8: PBE phonon dispersion spectra of (a) T1-FiM6 and (b) H1-AFM1.

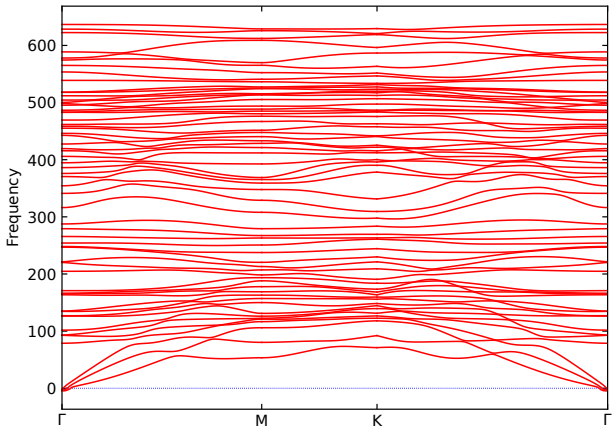

Figure S9: PBE phonon dispersion spectra of H1-AFM2.

S1.5 Influence of the Strain

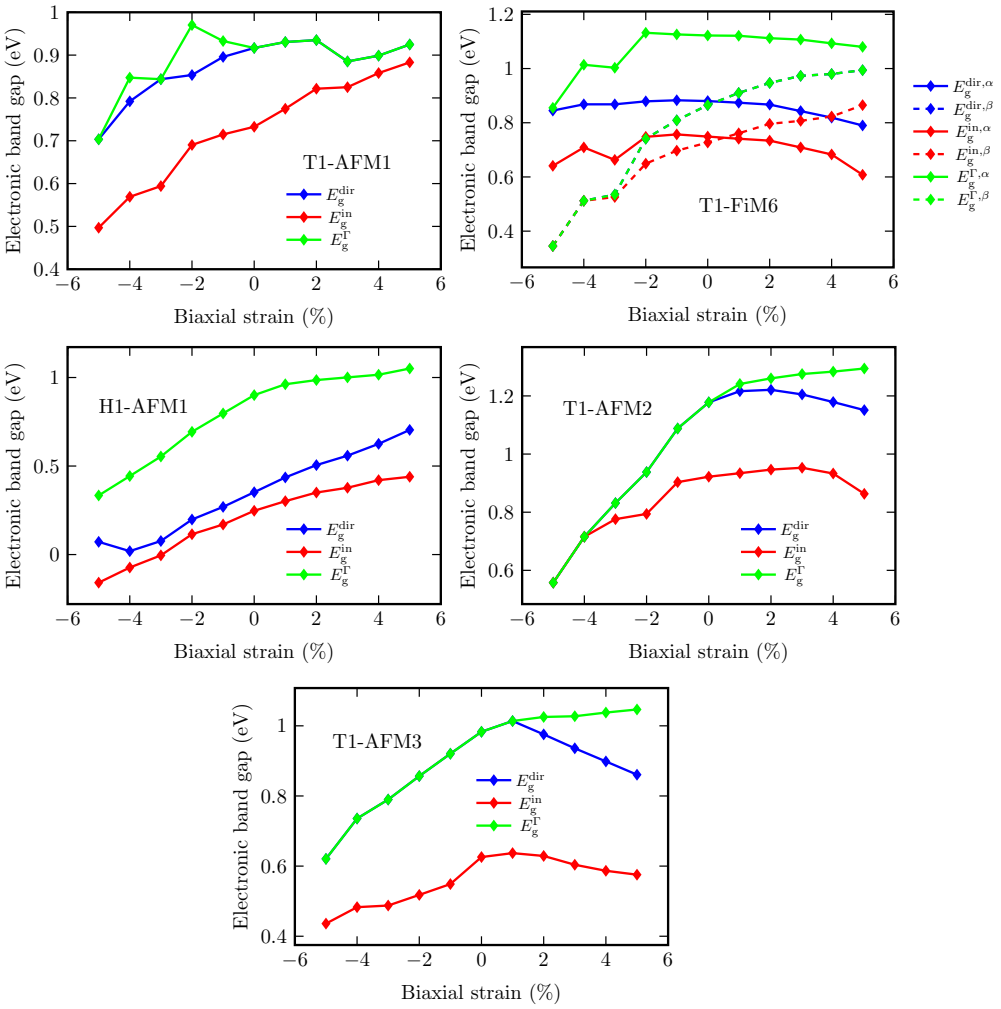

Figure S10: The effect of biaxial strain on the indirect (E_g^{in}), direct (E_g^{dir}) and Γ-point (E_g^{Γ}) electronic band gap in five isomers of Mn_2CO_2. For the FiM6 configuration the values for different spins α, β are presented.

S2 Electronic and Optical Properties

S2.1 Band structures

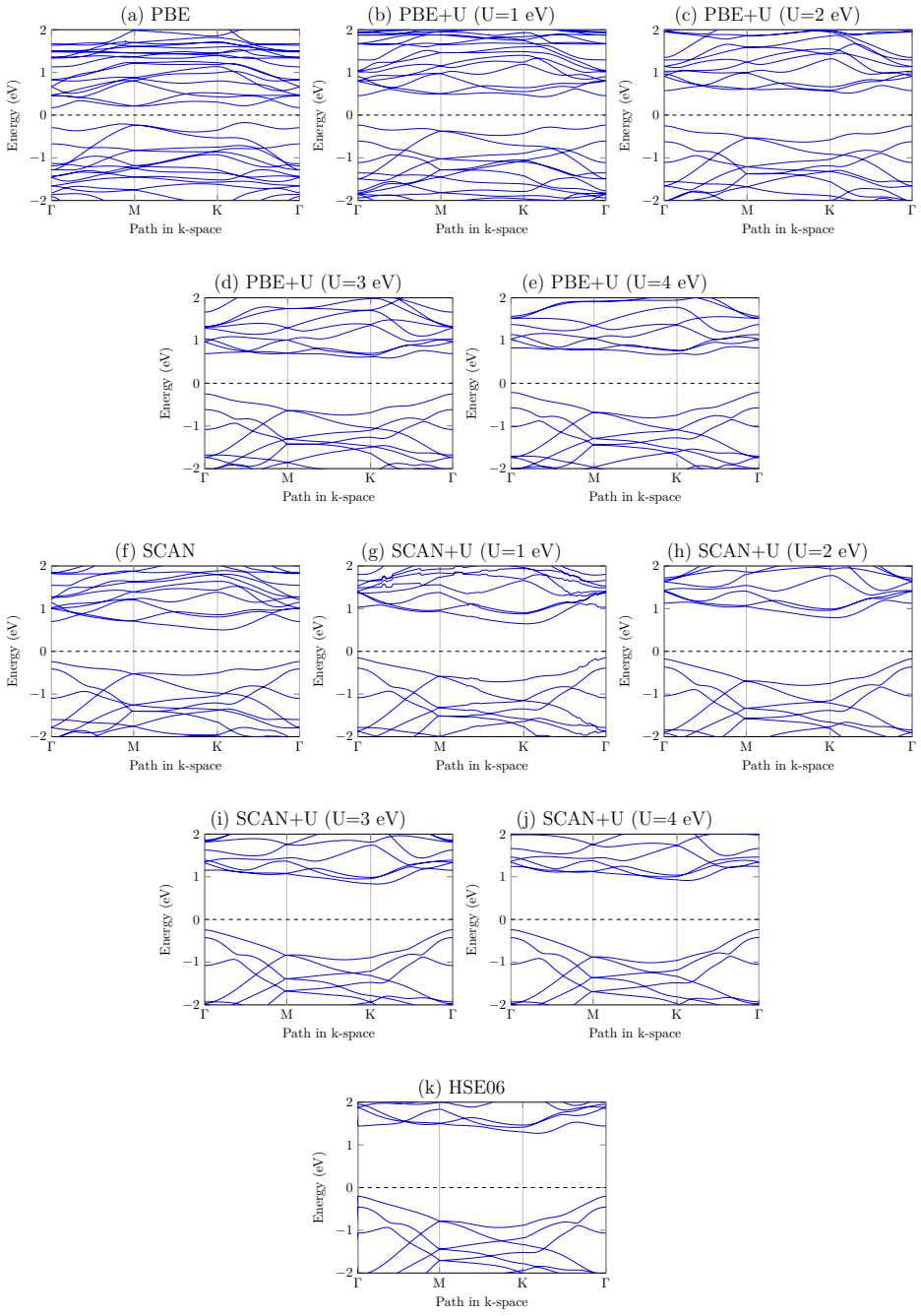

Figure S11: Band structures of Mn_2CO_2 MXene at various levels of computational DFT theory. (a) GGA PBE, (b)-(e) PBE+U (Hubbard correction), (f) meta-GGA SCAN, (g)-(j) SCAN+U, and (k) hybrid HSE06. Only bands of one spin are visible as the spin-polarized bands are identical near the Fermi level. Fermi energy is set to zero eV.

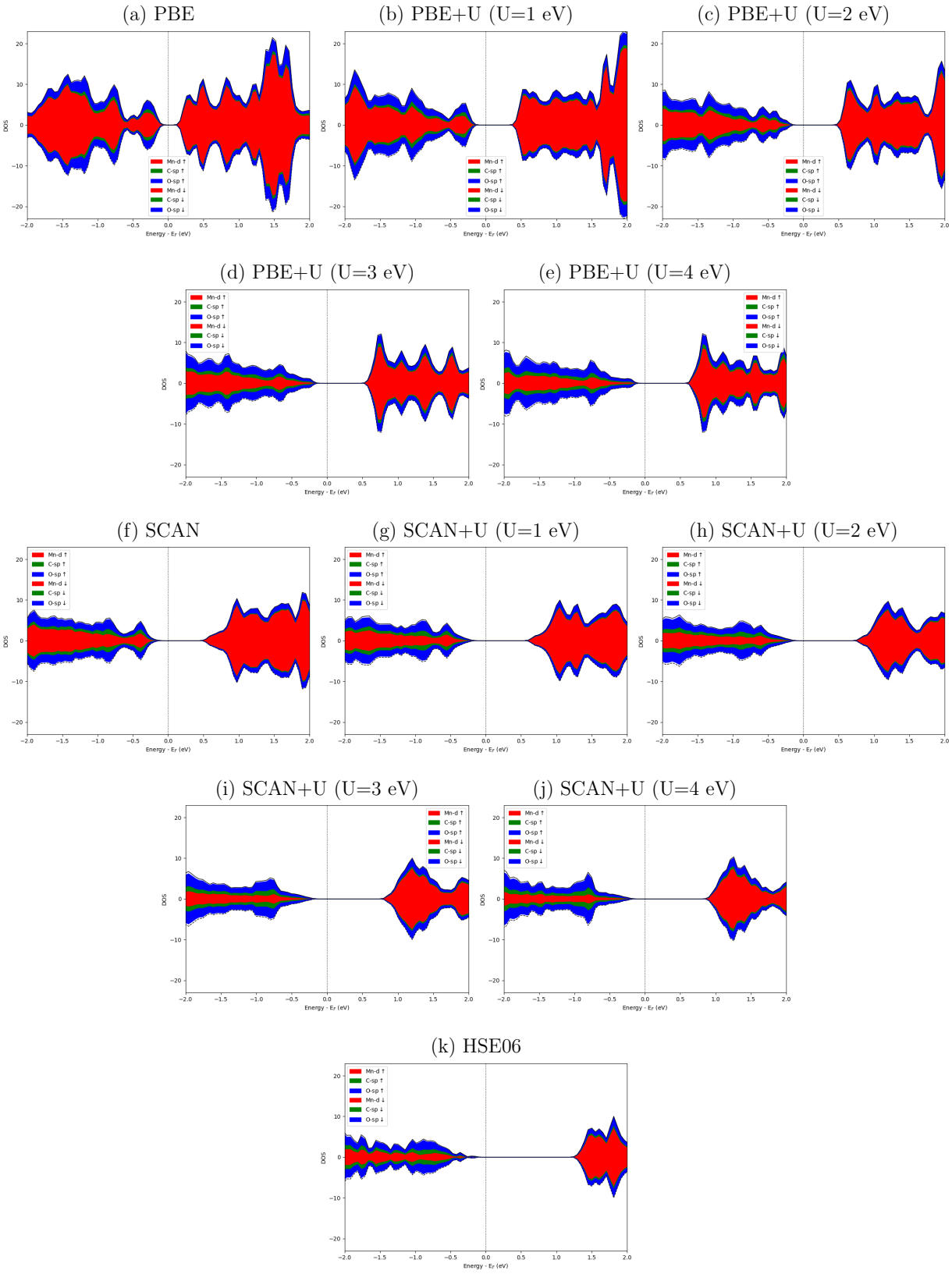

Figure S12: Partial density of states (PDOS) of the Mn_2CO_2 MXene at various levels of computational DFT theory. For C and O atoms, s and p states are considered, while d states are plotted for Mn atoms. The remaining s and p states for Mn atoms are uncolored and outlined by black lines. (a) GGA PBE, (b)-(e) PBE+U (Hubbard correction), (f) meta-GGA SCAN, (g)-(j) SCAN+U, and (k) hybrid HSE06. Fermi energy is in all figures set to zero eV.

Table S3: Electronic indirect (E_g^{indir}) and direct (E_g^{dir}) band gaps and magnetic moments m on Mn sites at different levels of DFT theory including density functionals PBE and SCAN with Hubbard correction U and hybrid functional HSE06.

Method	E_g^{indir} (eV)	E_g^{dir} (eV)	m (μ_B)
PBE	0.25	0.37	2.601
PBE + 1 eV	0.58	0.69	2.766
PBE + 2 eV	0.77	0.83	2.898
PBE + 3 eV	0.84	0.94	3.017
PBE + 4 eV	0.88	1.04	3.132
SCAN	0.73	0.92	2.728
SCAN + 1 eV	0.88	1.15	2.807
SCAN + 2 eV	0.99	1.28	2.904
SCAN + 3 eV	1.09	1.38	3.007
SCAN + 4 eV	1.17	1.47	3.118
HSE06	1.51	1.61	3.062

The electronic band gap obtained by using the Hubbard correction U = 3 eV, which was in previous studies (Hu et al. 2016, He et al. 2016, Dahlqvist et al. 2020) recommended for Mn-based MXenes, corresponds well with the native SCAN density functional without any empirical corrections. We, therefore, propose that the SCAN functional can describe the electronic band gap in Mn-based MXenes more accurately than the hybrid HSE06 density functional.

S2.2 Orbitals

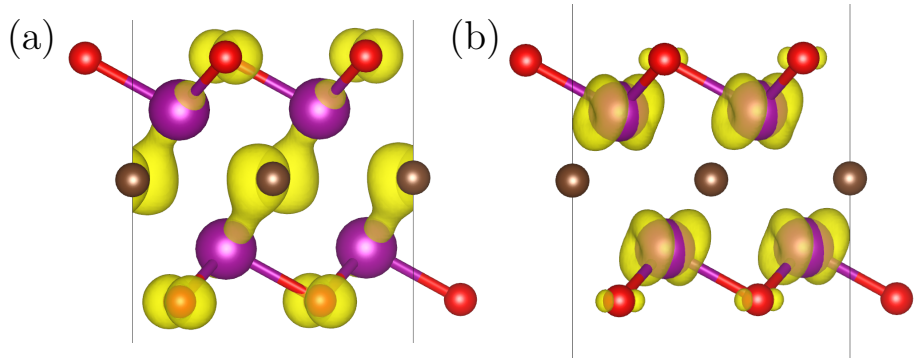

Figure S13: (a) The highest occupied orbital (HOMO) and (b) the lowest unoccupied orbital (LUMO) in Γ point for T1-AFM1.

S2.3 Convergence of GW and BSE Results

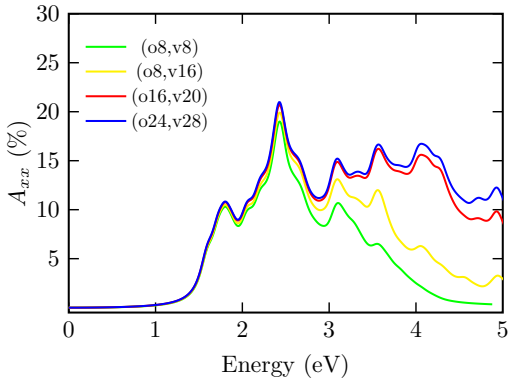

Figure S14: Convergence of optical absorption spectra ($A_{xx} = A_{yy}$) for T1-AFM1 Mn_2CO_2 MXene at the level of GW@SCAN + BSE with respect to the number of occupied (o) and virtual (v) bands used in the final BSE step. The results were obtained with $6 \times 6 \times 1$ k-point grid, $E_{\text{cut}}^{GW} = 200$ eV, $L_z = 20$ Å, $N_{\text{B}} = 3024$ and $N_\omega = 128$.

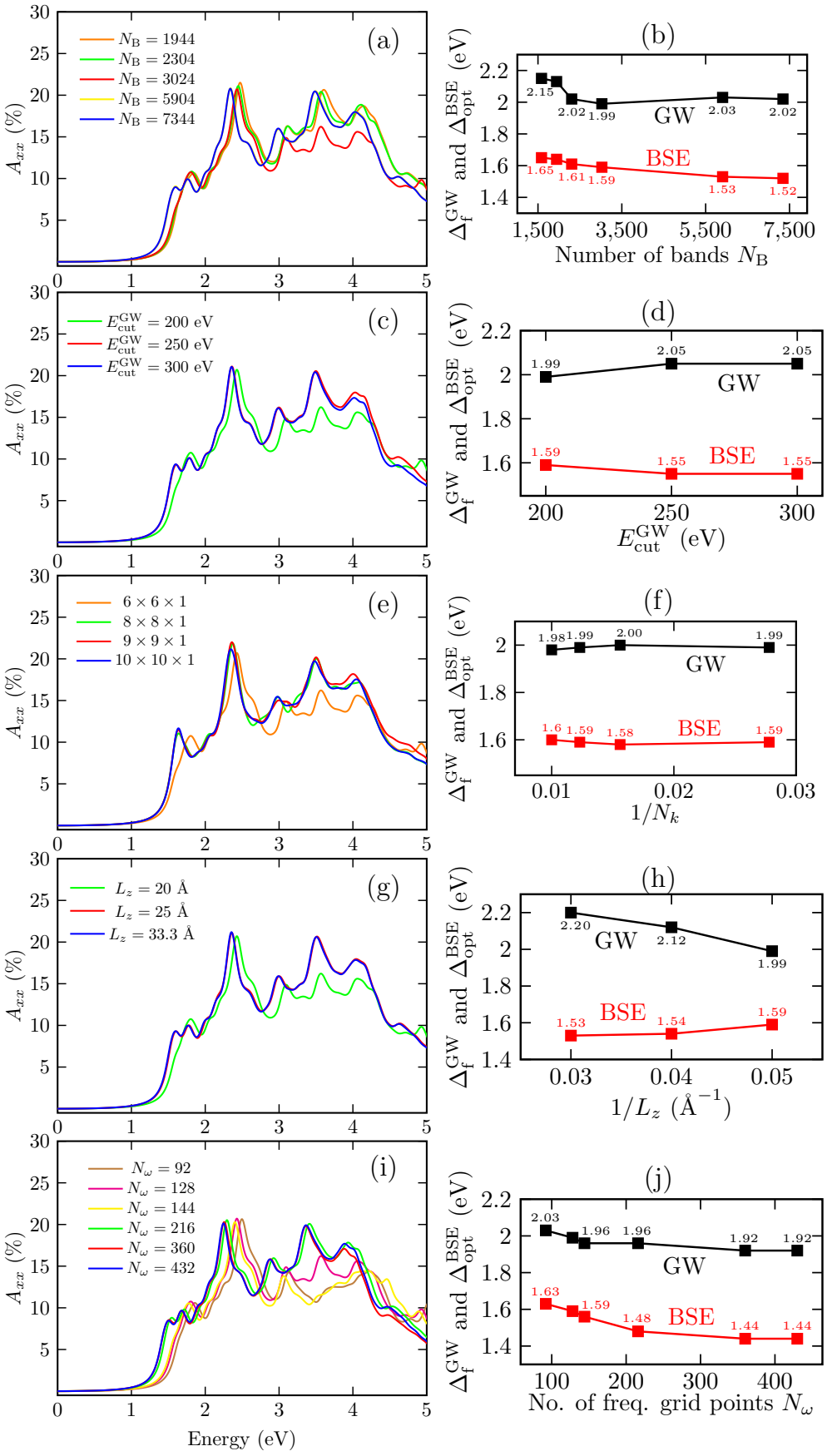

Figure S15: Convergence of optical absorption spectra ($A_{xx} = A_{yy}$), QP gap Δ_f^{GW} and optical gap Δ_{opt}^{BSE} for T1-AFM1 Mn_2CO_2 MXene at the level of GW@SCAN + BSE. Dependence of optical absorbance, direct Δ_f^{GW} and Δ_{opt}^{BSE} on (a)-(b) the number of bands N_B, (c)-(d) the GW cutoff energy E_{cut}^{GW}, (e)-(f) k-point grid density, (g)-(h) the height of the computational cell L_z and (i)-(j) the number of frequency dependent grid points N_ω. The initial settings for each calculation was $N_B = 3024$, $E_{cut}^{GW} = 200$ eV, $6 \times 6 \times 1$ k-point grid, $L_z = 20$ Å and $N_\omega = 128$ with each computational parameter being changed in its respective calculation.